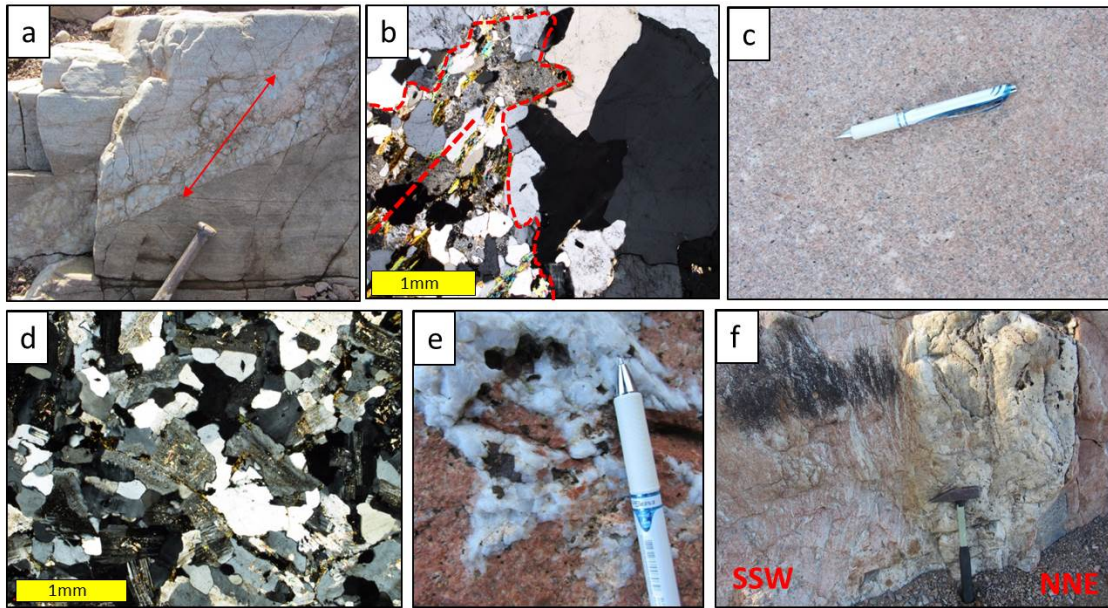


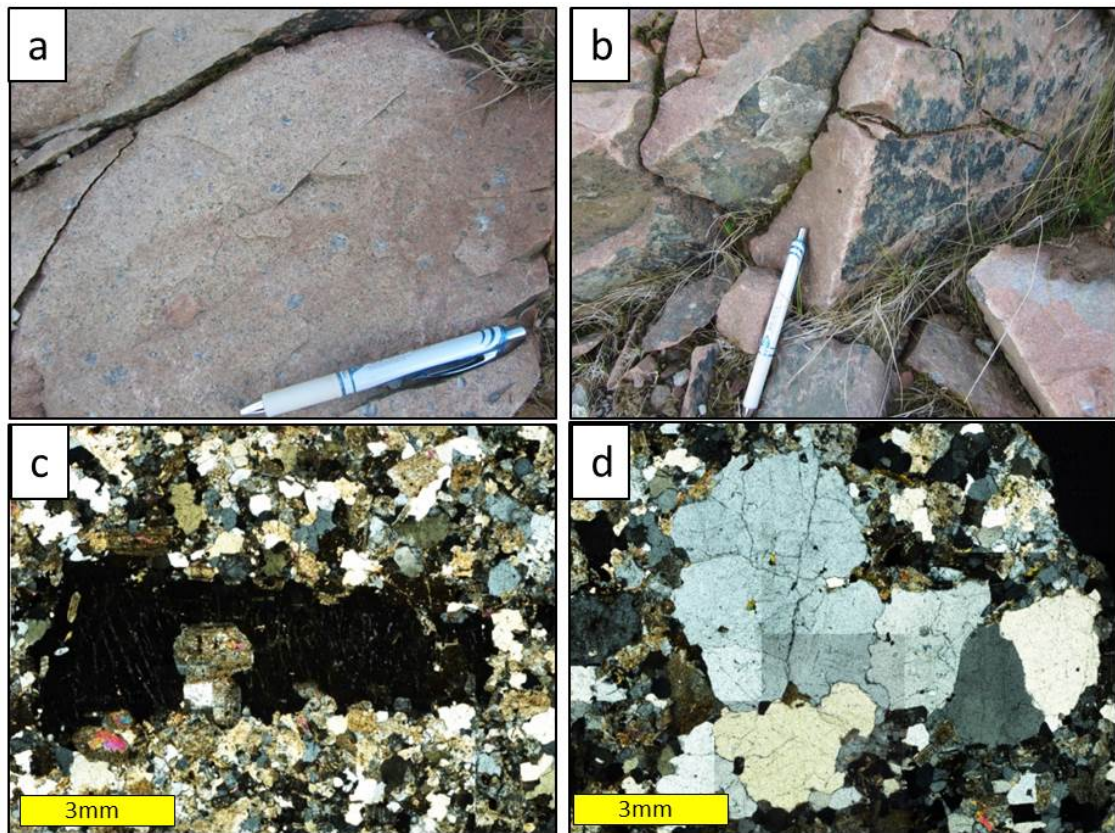
Appendices for Holdsworth et al. *Silurian-Devonian magmatism, mineralization, regional exhumation and brittle strike-slip deformation along the Loch Shin Line, NW Scotland*

Appendix A



The country rocks, Loch Shin granite and associated veins viewed in the field and thin section. **a)** Oblique view looking down onto undeformed granite pegmatite vein (077/55 NNW) cutting ACW of compositional banding in Moine psammites (100 metres to the SE of the Loch Shin granite (NC 5639 0613). Arrow shows inferred direction of vein opening based on offsets of thin semipelite layer. **b)** Thin section of undeformed granite pegmatite vein shown in (a) cross-cutting S0-S1-S2 fabric in Moine psammites (dashed yellow line). View in crossed polars, with igneous contact shown in red. **c)** Plan view in the field (NC 5631 0650) and **d)** in thin section (crossed polars) of typical undeformed Loch Shin granite (NC 5635 0631). **e)** Close-up plan view of irregular quartz-pyrite veins cutting Loch Shin granite (NC 5631 0650). **f)** Cross-section view of large NW-SE-trending quartz-galena veins (107/85N) cutting Loch Shin granite (NC 5630 0659).

Appendix B



Field and thin section views of the Grudie granite. **a)** Plan view of typical unfoliated Grudie granite with large pink K-feldspar and grey quartz phenocrysts/xenocrysts (NC 5268 0450). **b)** Oblique section view of slickenlined joints with chlorite and epidote mineralization (NC 5267 0444). **c)** Thin section of typical K-feldspar (in extinction) and **d)** polycrystalline quartz xenocryst/phenocrysts within Grudie granite (NC 5310 0427).

Appendix C

ZIRCON U-Pb ISOTOPE ANALYSIS

Sample, mineral separation and analytical protocols

A representative sample of Loch Shin granite from the SW west shore of Loch Shin (DS1-11; Fig. 2b, NC 5635 0625) was selected for Zircon U-Pb LA-ICP-MS geochronology. Zircons were separated from sample DS1-11 using heavy liquids and an isodynamic magnetic separator. The zircon fraction for analysis was handpicked under a binocular microscope and mounted in epoxy resin along with grains of the zircon reference material Temora 2 (Black *et al.* 2004). After polishing and carbon coating, cathodoluminescence (CL) images of the zircons were taken with a KeDev Centaurus CL detector housed on a JEOL 6060LV SEM at the University of Portsmouth (accelerating voltage = 15 kV).

Laser ablation (LA)-ICP-MS U-Pb isotope analyses were undertaken at the University of Portsmouth, using a New Wave 213 nm Nd:YAG laser coupled with an Agilent 7500cs quadrupole ICP-MS. Analytical protocols and instrument conditions are described in detail by Darling *et al.* (2012). Key points of the methodology are: (i) line-raster ablation (aspect ratio 1:1.5), in order to minimise time-dependent elemental fractionation; and (ii) external normalisation to the zircon standard Plesovice (Slama *et al.* 2008) using a 30 µm beam diameter. Laser beam diameters used on unknown zircons ranged from 30 to 15 µm, reflecting the scale of target domains within the crystals. Accuracy was monitored via analyses of the zircon reference materials Temora 2 and GJ-1. Eight analyses of Temora 2 (20 to 30 µm beam diameter) yield a U-Pb concordia age of 417.4 ± 3.5 Ma, and eight analyses of GJ-1 (30 µm beam diameter) yield a U-Pb concordia age of 606.6 ± 3.8 Ma: both of which are within uncertainty of the ID-TIMS reference ages for these materials (Black *et al.* 2004, Jackson *et al.* 2004).

Appendix D

RHENIUM-OSMIUM MOLYBDENITE GEOCHRONOLOGY

Mineral separation and analytical protocols

Molybdenite samples present in the area of the Grudie Granite were isolated using traditional methods of crushing, heavy liquids, and water flotation (Selby & Creaser, 2004). In contrast, given the minor abundance of molybdenite in the Loch Shin Granite sample (AF33-10), and to avoid losing molybdenite during crushing, the mineral separate was achieved using a room temperature HF dissolution of quartz protocol (Lawley & Selby, 2012).

The Re-Os analysis follows that outlined by Selby & Creaser (2004), which determines the Re and Os abundance of the molybdenite using isotope dilution negative thermal ionization mass spectrometry (ID-NTIMS). An aliquant of molybdenite, together with a known amount tracer solution (isotopically normal Os + ^{185}Re) are digested and equilibrated in a carius tube with 1ml 11N HCl and 3ml 15N HNO_3 for 24hrs at 220°C. Osmium is isolated and purified from the acidic solution using solvent extraction (CHCl_3) and micro-distillation methods. The Re is separated and purified using anion chromatography. The separated Re and Os were loaded on Ni and Pt wire filaments with BaNO_3 and BaOH activators, respectively, and analyzed for their isotope compositions using NTIMS via static Faraday collection. Analytical uncertainties are propagated and incorporate uncertainties related to Re and Os mass spectrometer measurements, blank abundances and isotopic compositions, spike calibrations, and reproducibility of standard Re and Os isotope values. The molybdenite analyses of this study were conducted during the same period as those of Lawley & Selby (2012). This study reported Re and Os blanks of <4 and 1 pg, respectively, with the $^{187}\text{Os}/^{188}\text{Os}$ of the blank being 0.25 ± 0.02 (n = 2). Further, Re-Os model ages determined using the ^{187}Re decay constant of $1.666 \times 10^{-11} \text{ a}^{-1}$ (Smoliar *et al.*, 1996) of molybdenite reference materials (NISTRM8599 = 27.6 ± 0.1 and 27.6 ± 0.1 Ma; HLP-5 = 220.0 ± 0.9 Ma), which are in good agreement with their accepted values determined at other laboratories and those previously reported at Durham University (Markey *et al.*, 1998, 2007; Porter & Selby, 2010).

Appendix E

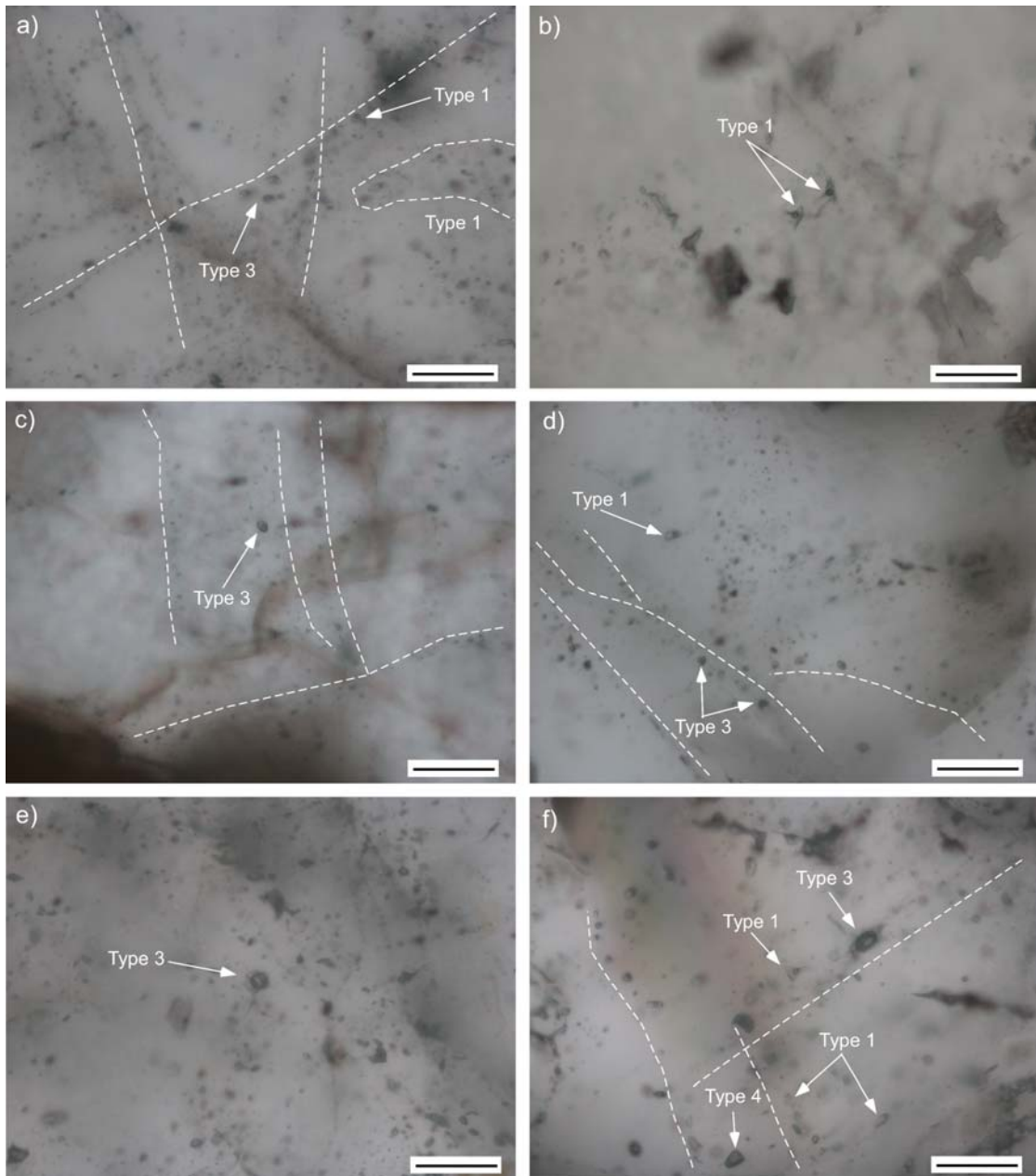
FLUID INCLUSION ANALYSIS

Analytical protocols

Microthermometric analysis was performed on doubly polished wafers (~100 mm thick) using a Linkam THMGS 600 heating freezing stage, mounted on an Olympus transmitted polarised light microscope. The instrument is equipped with a range of special long working distance objective lenses ranging up to 100x magnification. Calibration of the stage was performed using synthetic fluid inclusion standards (pure CO₂ and H₂O). Precision is ± 0.5°C at 300°C and ± 0.2°C at -56.6°C. Following procedures outlined by Shepherd *et al.* (1985), the temperature of first ice melting T_{FM}, the temperature of last ice melting T_{LM} and the temperature of homogenisation T_H were measured in quartz hosted two-phase liquid+vapour inclusions in all wafers (Fig. 9a). Fluid salinities were calculated using T_{LM} and the equations of Bodnar (1993). In addition, clathrate melting temperatures recorded in three-phase (L_{H2O}+L_{CO2}+V_{CO2}) aqueous-carbonic inclusions were used with the equations of Duan *et al.*, (1996) to calculate their fluid salinities (Fig.9b).

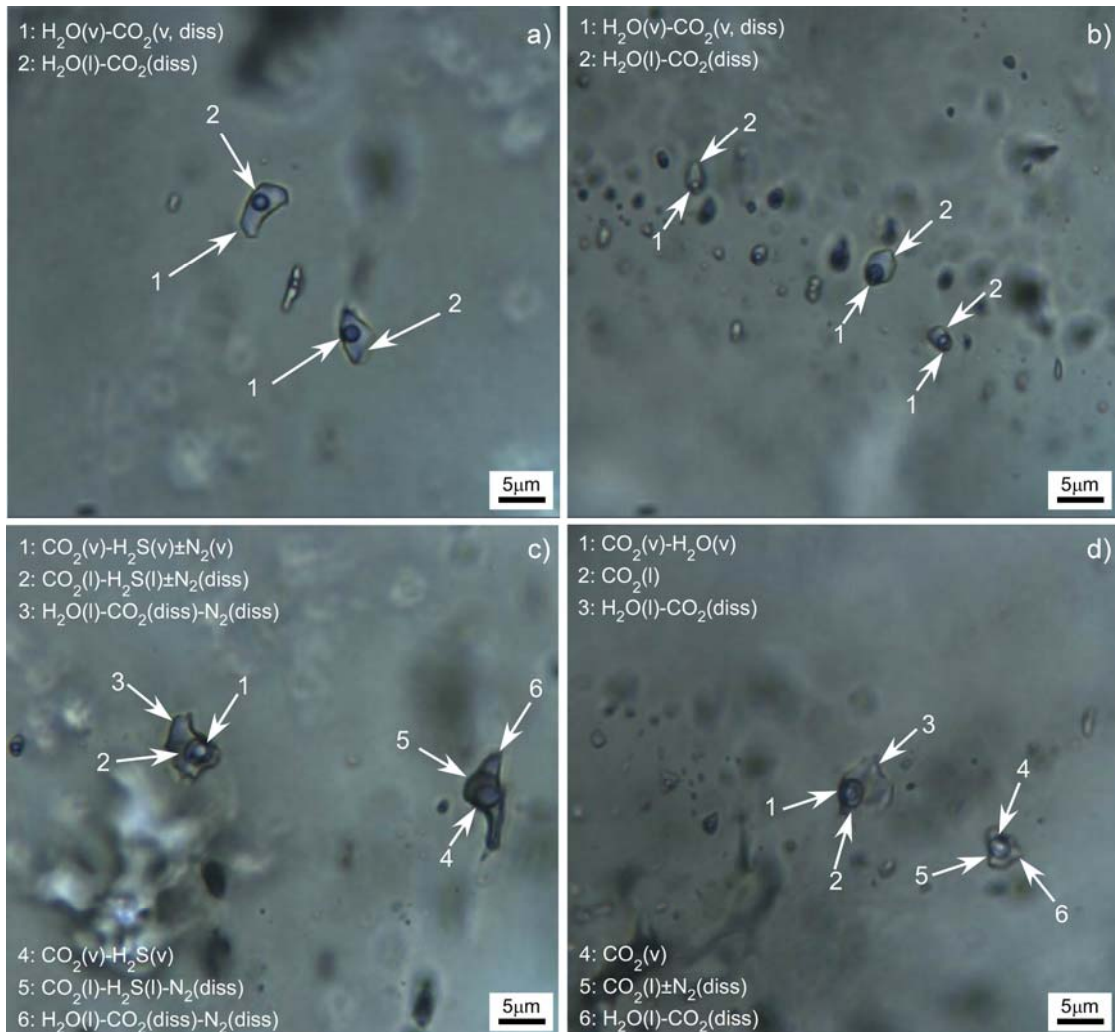
Laser Raman Microspectroscopy (LRM) of fluid inclusions was performed using a Horiba LabRam II laser Raman spectrometer. The instrument is equipped with a 600 groove mm⁻¹ diffraction grating, a confocal and optical filter system, a Peltier-cooled CCD detector (255 x 1024 pixel array), and is coupled to an Olympus BX51 microscope. Fluid inclusion gas and liquid phases were analysed at room temperature using a 532 nm laser focused through either a 50x or 100x microscope objectives. The spatial resolution of the 532 nm laser at the sample was approximately 2 µm. Individual analyses were performed for between 10 to 60 seconds over the spectral range 1100 cm⁻¹ to 4200 cm⁻¹. The number of spectral accumulations per analysis typically ranged between 2 to 5 in order to maximize the signal-to-noise efficiency of the spectrometer. Calibration of the instrument was routinely performed between analyses using the Raman peak of a pure silicon standard (520.7 cm⁻¹). Spectral uncertainty associated with the generation of Raman peak positions is estimated to be ± 1.5 cm⁻¹ (2σ; 0.3%) based on replicate analyses of the standard.

Appendix F



Photographs of fluid inclusions (FI) trails from samples AF33-10 – Loch Shin Granite (**a,b**); AF35-10 (**c,d**) and AF02-10 (**e,f**) both from Gruide Granite. Scale bar = 50 µm.

Appendix G



Photomicrographs of Type 1 and Type 3 inclusions within quartz grains in sample AF35-10 (Gruidé granite) analysed under Laser Raman Spectroscopy. Type 1 two-phase liquid-rich aqueous inclusions distributed in isolated cluster **(a)** and trails **(b)**. Type 3 three-phase aqueous-carbonic inclusions distributed in clusters **(c and d)**.

**Appendix H:
Re-Os data for molybdenite from Lagalochan Porphyry Cu-Mo system**

Sample	location	wt (g)	Re(ppm)	±	¹⁸⁷ Re(ppm)	±	¹⁸⁷ Os(ppb)	±	Age	±
RO562-4_RC843047	Hole LD13-1A: 77.45-77.55m depth: 56deg 15' 19.0" N and 05deg 25' 41.1"	0.012	1215.9	5.5	764.2	3.5	5405.0	22.1	423.0	1.7
RO562-5_RC843048	Hole LD13-1A: 115.80-115.90m depth: 56deg 15' 19.0" N and 05deg 25' 41.1"	0.011	254.4	1.2	159.9	0.8	1131.5	4.9	423.2	1.7

Appendix I: Coire Buidhe Fluid Inclusions

Three types of fluid inclusion (Type 1, 2 and 3) were identified in vein quartz from Coire Buidhe (CB1A, B; see Porter & Selby 2010 for sample details), based on their morphology, composition and phase relations at room temperature. Type 1 inclusions are three-phase (liquid H₂O + liquid CO₂ + CO₂ vapour) at room temperature (~25°C). They are found as isolated inclusions, randomly distributed throughout the quartz, and appear to be primary or pseudosecondary in origin. On cooling, the carbonic phase in Type 1 inclusions freezes at ~ -120°C. Melting of the carbonic phase in all inclusions occurs between -57.1 and -56.5°C. Most melting temperatures are close to the triple point of CO₂ (-56.6°C), indicating that the inclusions contain almost pure CO₂. This is confirmed by Laser raman analysis that shows the volatile phase contains < 97.7% CO₂, with minor CH₄, N₂ and H₂S. Clathrate melting, in the presence of liquid CO₂ occurred between 3.7 and 6°C and yields salinities between 7.1 and 11.1 eq. wt% NaCl using the equation of Duan *et al.* (1995) and the software program CLATHRATES (Bakker, 1997). Homogenisation of CO₂ (to the liquid phase) occurs between 27 and 30.4°C, indicating a CO₂ phase density of 0.57 to 0.68 g/cc. Total homogenization to the liquid phase occurs between 291 and 353°C. Type 2 aqueous inclusions are two-phase (liquid + vapour) inclusions and occur along healed microfractures that crosscut quartz grain boundaries. The temperature of first ice melting (T_{FM}) takes place between -20.7 and -23.8° C, close to the eutectic temperature of the H₂O-NaCl-KCl system (-22.9°C). T_{LM} values are between -3.1 and -5.1°C. Clathrate melting between 1.2 and 2.9°C was observed in some Type 2 inclusions. This indicates the presence of non-aqueous phases in Type 2 inclusions. Laser raman analysis of Type 2 inclusions confirmed that the vapour phase contains > 98% CO₂ with minor amounts of CH₄, N₂ and H₂S. Clathrate melting temperatures have been used to calculate salinities of 5 to 5.2 eq. wt% NaCl using software program CLATHRATES (Bakker, 1997). Type 2 inclusions homogenised to the liquid phase (L + V → L) between 261.9°C and 282.9°C.

Type 3 inclusions are found in trails along annealed microfractures, that are occasionally crosscut trails of Type 2 inclusions. First ice melting temperatures were recorded between -21.3 and -24.6°C. T_{LM} values lie between -2.7 and -4.9°C and

correspond to salinities of 4.5 to 7.7 eq. wt% NaCl (Bodnar, 1993). Type 3 inclusions homogenized to the liquid phase (L + V → L) between 165.5 and 218°C.

Additional References Cited in Appendices

- Bakker, R.J., 1997. Clathrates: computer programs to calculate fluid inclusion V-X properties using clathrate melting temperatures. *Computers & Geosciences*, **23**, 1-18.
- Black, L.P., Kamo, S.L., *et al.* 2004. Improved ²⁰⁶Pb/²³⁸U microprobe geochronology by the monitoring of a trace-element-related matrix effect; SHRIMP, ID-TIMS, ELA-ICP-MS and oxygen isotope documentation for a series of zircon standards. *Chemical Geology*, **205**, 115-140, doi: 10.1016/j.chemgeo.2004.01.003.
- Bodnar, R.J., 1993. Revised equation and table for determining the freezing point depression of H₂O-NaCl solutions. *Geochimica Cosmochimica Acta*, **57**, 683-684.
- Duan Z.H., Møller N., Weare J.H. 1995. Equation of state for the NaCl-H₂O-CO₂ system: prediction of phase equilibria and volumetric properties. *Geochim Cosmochim Acta*, **59**, 2869-2882
- Duan, Z., Moller, N. & Weare, J.H., 1996. A general equation of state for supercritical fluid mixtures and molecular dynamics simulation of mixture PVTX properties. *Geochimica Cosmochimica Acta*, **60**, 1209-1216
- Jackson, S.E., Pearson, N.J., Griffin, W.L. & Belousova, E.A. 2004. The application of laser ablation-inductively coupled plasma-mass spectrometry to in situ U-Pb zircon geochronology. *Chemical Geology*, **211**, 47-69, doi: 10.1016/j.chemgeo.2004.06.017.
- Markey, R., Stein, H., Hannah, J.L., Zimmerman, A., Selby, D., Creaser, R.A., 2007. Standardizing Re-Os geochronology: a new molybdenite Reference Material (Henderson, USA) and the stoichiometry of Os salts. *Chemical Geology*, **244**, 74-87.
- Markey, R., Stein, H., Morgan, J., 1998. Highly precise Re-Os dating for molybdenite using alkaline fusion and NTIMS. *Talanta* **45**, 935-946.
- Slama, J., Kosler, J., *et al.* 2008. Plesovice zircon - A new natural reference material for U-Pb and Hf isotopic microanalysis. *Chemical Geology*, **249**, 1-35, doi: 10.1016/j.chemgeo.2007.11.005.
- Smoliar, M. I., R. J. Walker, *et al.* (1996). "Re-Os isotope constraints on the age of Group IIA, IIIA, IVA, and IVB iron meteorites." *Science*, **271**: 1099-1102.